J. Fluid Mech. (1965), *vol.* 23, *part* 1, *pp.* 173–183
Printed in Great Britain

Luminescence in supersonic swirling flows

By Z. LAVAN
IIT Research Institute, Chicago, Illinois
AND A. A. FEJER
Illinois Institute of Technology, Chicago, Illinois

(Received 19 October 1964 and in revised form 15 March 1965)

A luminescent region was observed near the axis of a cylindrical duct confining a supersonic swirling air flow at ambient temperature. The luminescence was identified as a glow discharge induced by a strong internal electric field, which was produced by condensed water droplets impinging on the duct wall.

1. Introduction

The vortex tube was discovered in 1931 by Ranque. In this simple flow device (Ranque 1933), air introduced tangentially at one end of a cylindrical duct separates into two streams of different temperatures. The low-temperature stream occupies the axial core, the warmer stream the outer region of the duct. Following Ranque's discovery, swirling flows of subsonic axial velocities were the subject of many investigations (extensive bibliographies have been compiled by Westley 1954, Gartshore 1962 and Dobratz 1964). In extending these studies to flows with supersonic axial velocities, the authors observed an unexpected glow discharge in the central region of the tube. A discussion of this phenomenon is presented in the following paragraphs.

2. The flow

The experimental apparatus used to produce the flow (figure 1) consisted of a radial entrance section followed by a convergent-divergent cylindrical nozzle, and a transparent cylindrical duct (3 in. inside diameter) leading to a 24 ft. diameter vacuum sphere. The entrance section was equipped with a cascade of adjustable pre-rotation vanes that imparted a swirl to the entering ambient air.

The experimental investigations involved mass flow and wall static-pressure measurements, probing of the flow field and flow visualization techniques. Streamline patterns in the inlet section were explored by means of tufts and surface coatings of lampblack. In addition, black ink injected through a small hole in the duct wall upstream of the test section produced a spiraling trace on the wall. For a fixed setting of the pre-rotation vanes the pitch of this spiral decreased sharply with an increase in Mach number when the axial flow was supersonic, but changed only slightly with Mach number when the flow was subsonic. This is due to the fact that in the case of supersonic axial flow, the tangential velocity is largely determined by the vane setting, while the axial velocity is strongly affected by the area ratio of the convergent-divergent nozzle.

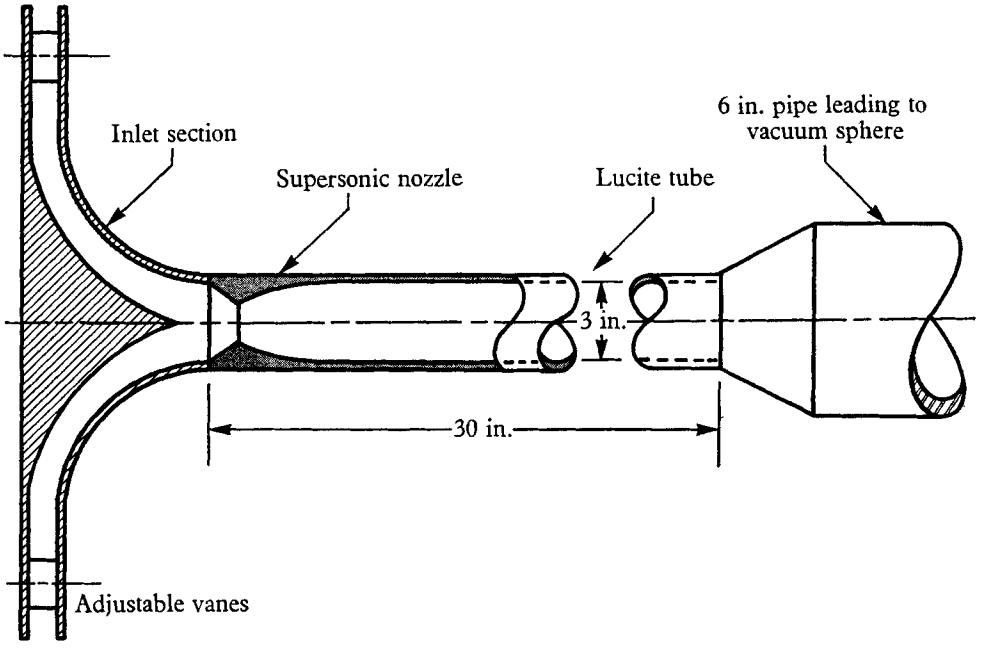

FIGURE 1. Schematic diagram of the inlet section, supersonic nozzle and cylindrical test section.

Shadowgraph observations showed that the swirling flow in the test section was indeed supersonic. The swirl angle was indicated by the orientation of the bow shock around a small probe having a spherical tip.

In surveying the pressure in the interior of the tube, the swirling flow was found to be very sensitive to disturbances caused by the presence of the probe. This effect was minimized when the probe was oriented along a radius and was of sufficient length to span the tube cross-section. This probe (figure 2(*b*)) was made of two 0·064 in. diameter stainless-steel tubes connected by a short brass insert. Two 0·008 in. holes drilled radially in this insert at an included angle of approximately 80° were vented to opposite ends of the insert through 0·013 in. axial holes. The flow direction was established by rotating the probe until equal pressures were registered at the two ends. The stagnation pressure was then obtained by rotating the probe through half the included angle between the holes. The static pressure was determined from the stagnation pressure, the pressure at a pre-selected angular position of 40° from the direction of flow, and calibration curves relating the pressure at this position to the Mach number. The calibration curves were practically independent of the Reynolds number, since the flow around the probe was always subcritical (Howard 1953).

The temperature probe (figure 2(*a*)) employed in this study was of the same external geometry as the pressure probe. It consisted of a chromel-alumel junction with 28-gauge leads passing through a 0·050 in. two-hole ceramic cylinder which was housed in a stainless-steel tube of 0·064 in. outside diameter. A section of the wall of this tube was cut out to expose the thermocouple junction

and to provide a shielded region for the stagnant air. This thermocouple has a fast response time and a good recovery factor for both subsonic and supersonic flows (Stickney 1955).

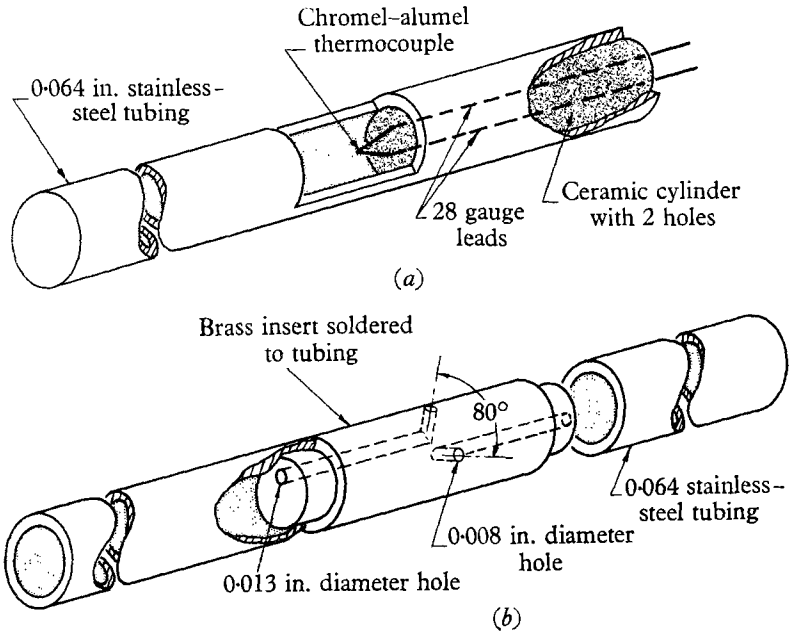

FIGURE 2. Temperature and pressure probes (overall length of probe is 8 in.). (*a*) Stagnation temperature probe. (*b*) Two-hole pressure probe used for flow direction and pressure measurements.

The flow pattern in the present test exhibited a similarity to the well-known structure of swirling flows predicted by potential theory, i.e. a potential vortex annulus (vr = const.) in the outer region, and a low-pressure central core with solid body rotation (v/r = const.). Typical surveys of static and total pressures, stagnation temperatures, tangential and axial velocities and swirl angles are shown in figures 3 and 4. They were obtained using a Mach 2 nozzle at an ambient temperature, T_0, of 79 °F and a pressure, P_0, of 29·95 in. Hg. The swirl angle, θ, and the tangential velocity, V_θ, (figure 3) are seen to increase linearly with radial distance near the axis, peaking at a radius of approximately 0·8 in. and then decreasing slowly toward the wall. The maximum swirl angle was 28° and the angle of the coloured trace on the wall described earlier was 19°. The axial velocity, V_x, is seen to have a dip near the axis which is associated with an increase in pressure and a rapid decay of the tangential motion in the direction of the flow. This behaviour was also encountered by the authors in the numerical solution of the Navier–Stokes equations for laminar incompressible swirling flow in the entrance region of circular ducts.

The radial distribution of stagnation temperature is shown in figure 4, where $T_t - T_0$ is the difference between the local stagnation temperature and the ambient temperature. The maximum temperature difference was approximately

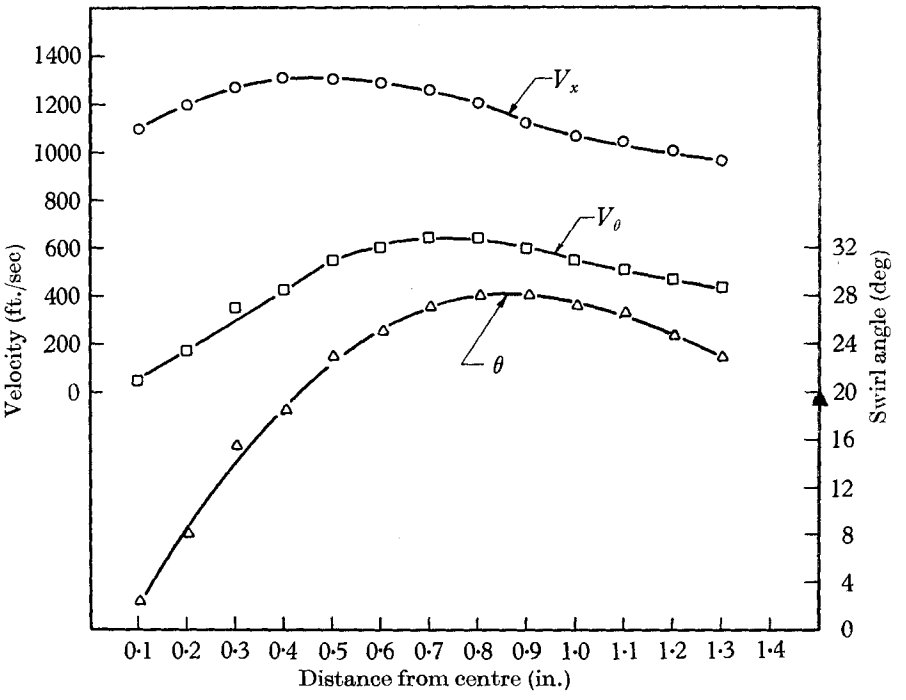

FIGURE 3. Radial distribution of velocities and swirl angle.

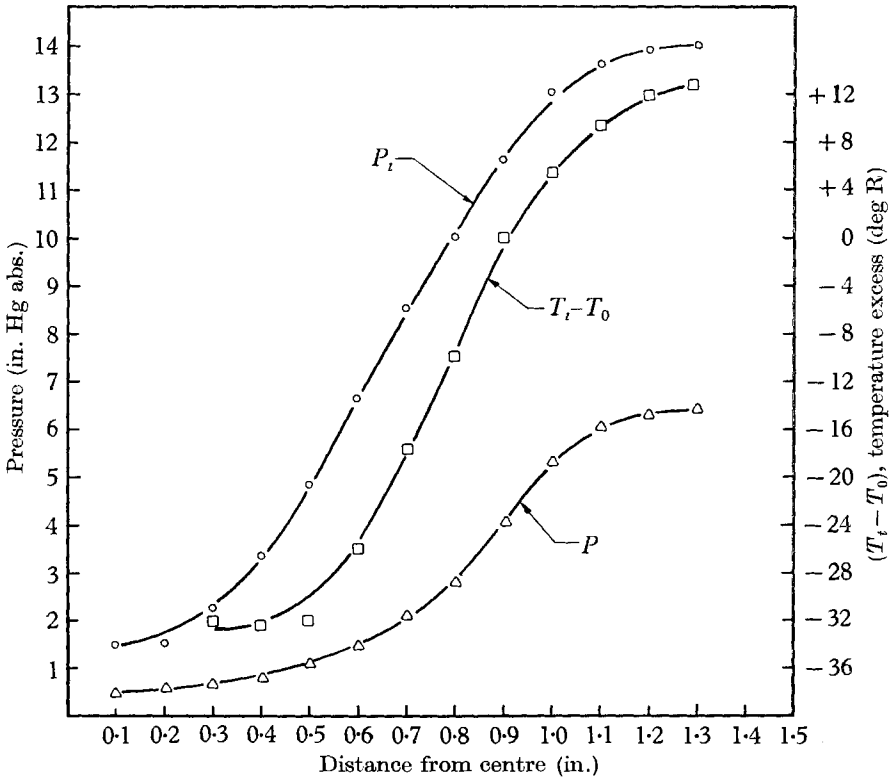

FIGURE 4. Radial distribution of pressure and temperature excess.

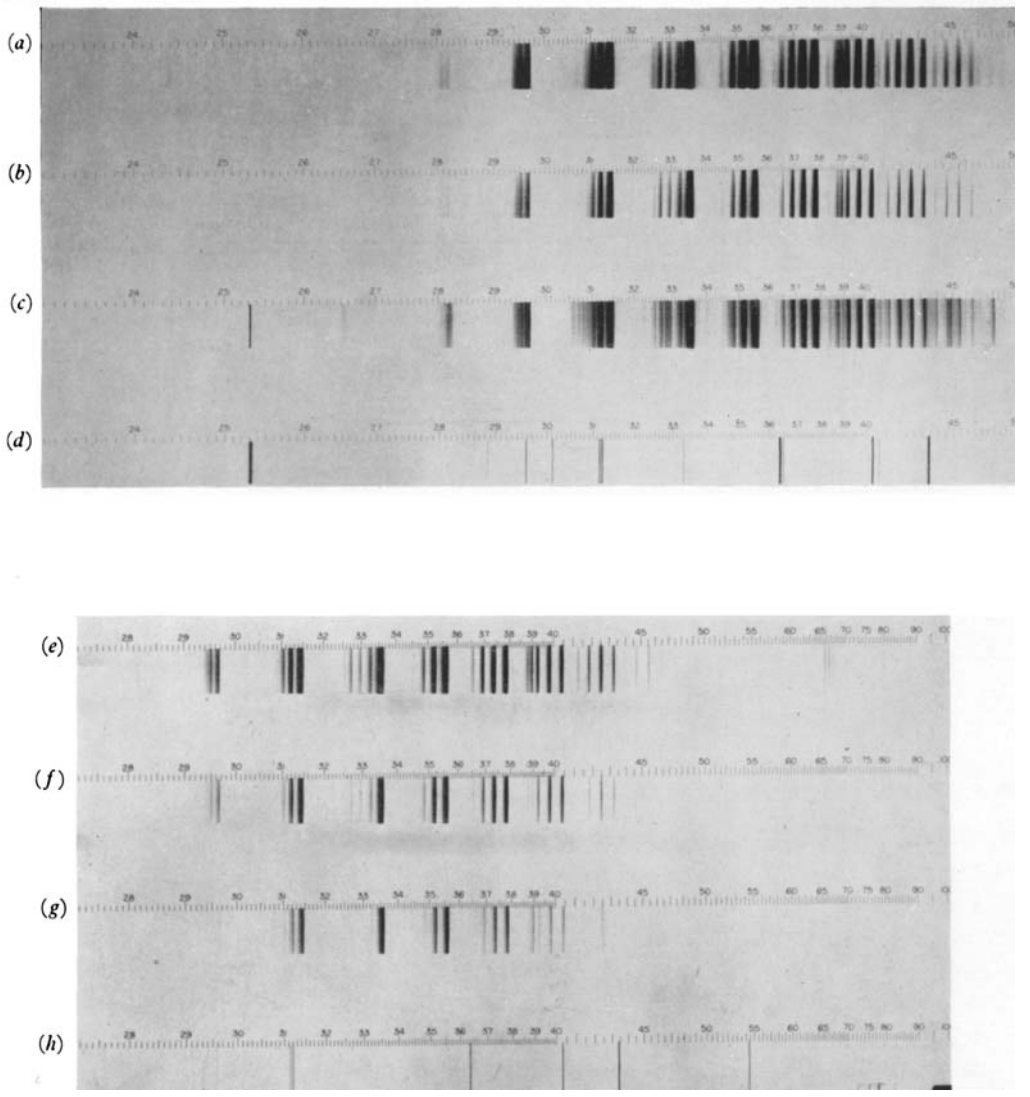

FIGURE 5. Spectrograms. (*a*) Swirling flow (slit, 350μ; exposure time, 6 min). (*b*) Swirling flow (slit, 100μ; time, 100 sec). (*c*) N_2 discharge tube (slit, 100μ; time, 80 sec). (*d*) Standard mercury arc. (*e*) Swirling flow (slit, 100μ; time, 10 min). (*f*) Swirling flow (slit, 100μ; time, 60 sec). (*g*) Air discharge tube (slit, 100μ; time, 4 min). (*h*) Standard mercury arc.

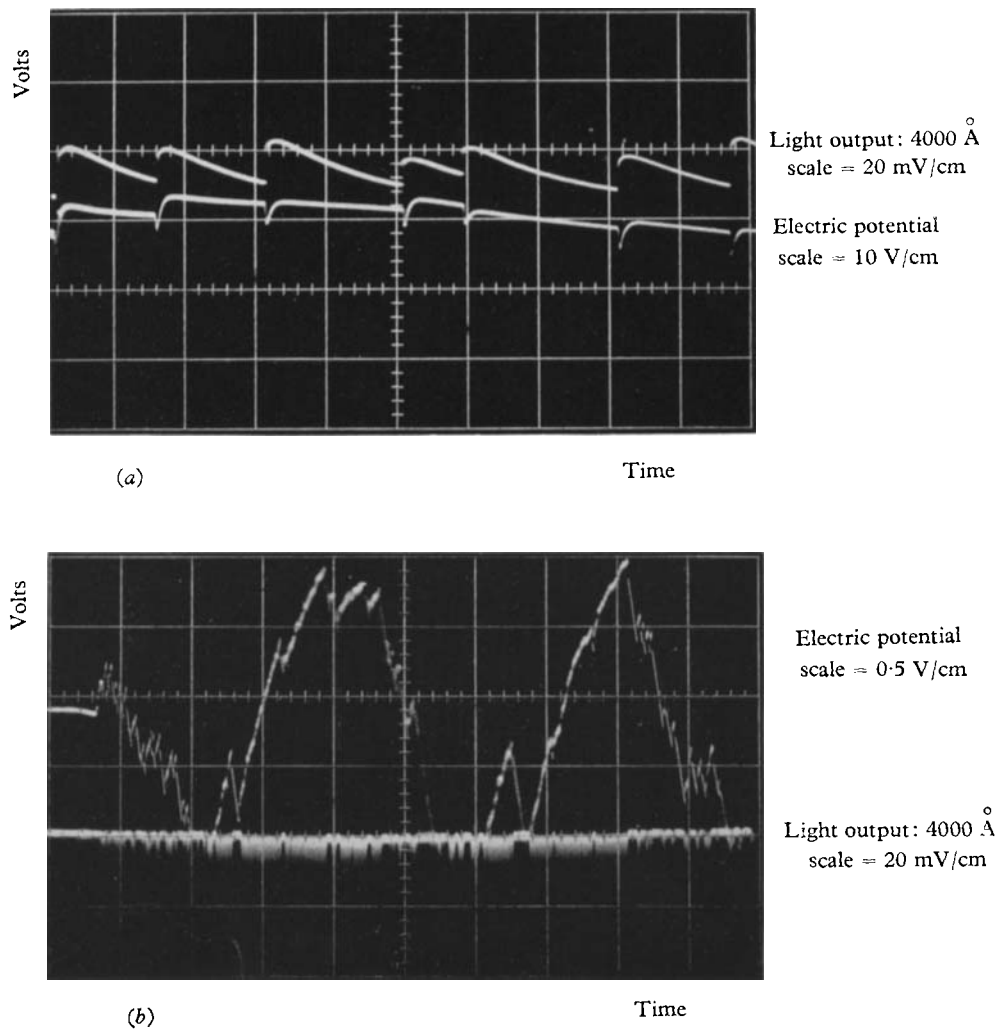

FIGURE 9. Oscilloscope traces of electric potential and light output. (*a*) Sweep = 20 μsec/cm. (*b*) Sweep = 2 sec/cm.

48 °F, with the temperature near the axis being 43 °F. The stagnation and static pressures, P_t and P, are also shown in figure 4. The static pressure increases from 0·75 in. Hg near the axis to approximately 6·5 in. Hg near the wall. The shape of this curve is strongly reminiscent of the pressure distribution of a potential vortex model. (See, for example, Milne-Thompson 1957.)

The mass flow under these conditions was 0·73 lb./sec, and it increased to 1·39 lb./sec when the swirl was removed, suggesting that in supersonic flows, swirl may be used to control the mass flow.

When a dielectric test section (glass, Lucite) was used in combination with a Mach 2 nozzle and with relatively high swirl velocities, the central region of the flow became luminescent. This region was cylindrical in shape, approximately 1 in. in diameter and extended along the entire length of the test section. The luminescence increased uniformly with swirl intensity and with the specific humidity of the ambient air, and it decreased when the axial Mach number was raised or lowered. When the dielectric duct was replaced by one made of a conducting material, no luminescence was observed.

3. Spectroscopic investigations

The glow was at first examined with a Hilger medium quartz spectroscope. Spectrograms were obtained at various flow conditions through quartz windows at three axial locations. The spectra at these locations were of different intensities but revealed identical structures characteristic of the emission of excited molecular nitrogen. Both the ultra-violet and infra-red spectra were recorded using two types of photographic plates (Kodak 103-0 and 1-F); exposure times were varied from 1 to 10 min, yielding clear records of systems of different intensities. Typical spectrograms of the vortex glow are shown in figures 5(*a*), (*b*), (*e*) and (*f*) (plate 1). Nitrogen at 0·5 torr and air at 1·5 torr discharge spectra are shown in figures 5(*c*) and (*g*) (plate 1) for comparison. (The 2537 Å line appearing in 5(*c*) is a mercury resonance line which undoubtedly is due to mercury vapour trapped in the discharge tube during evacuation.) The spectra were calibrated with the aid of a standard mercury arc spectrum (figure 5(*d*) and (*h*), plate 1).

The spectroscopic observations reveal an intense emission spectrum of the second positive system of N_2 and considerably weaker spectra of its first and fourth positive systems. The wavelength of the observed band heads and the corresponding vibrational quantum numbers are listed in table 1. The energy levels of the systems involved (Herzberg 1950) are shown diagramatically in figure 6; their upper state and transition energies are given in table 2. The average lifetime of excited N_2 molecules in the lower state of the first positive system ($A^3\Sigma_u^+$) is approximately 0·1 sec, while that of those in the higher states is 10^{-8} to 10^{-10} sec. Thus, one may conclude that the higher states must be excited locally while molecules in the $A^3\Sigma_u^+$ meta-stable state could be brought conceivably from an upstream source by the flow. In this case, excitation from $A^3\Sigma_u^+$ to the higher states would require transition energies up to 5·2 eV as can be seen from figure 6. Such an energy increase cannot be achieved by a single molecular collision since the average translational energy at the existing temperature is only 1/30 eV

(assuming a Maxwell–Boltzmann distribution, $\frac{3}{2}KT$). Excitation by a step up in the vibrational levels due to a series of consecutive collisions is also impossible in view of the extremely high de-excitation probability at test conditions.

The agreement between the observed spectrum and the spectrum of the positive column of an N_2 discharge tube (Pearse & Gaydon 1941) strongly suggests that the phenomenon is an active discharge due to an electric field. In such a discharge, electrons may acquire energies of the order of 10 eV and could therefore readily excite the nitrogen molecules to the observed levels. Electric field measurements and monochrometer observations reported in the following paragraphs confirm this hypothesis.

The first positive system $B^3\pi_g \rightarrow A^3\Sigma_u^+$

λ	v', v''
6704·8	5, 2
6623·6	6, 3
6544·8	7, 4
6468·5	8, 5

The second positive system $C^3\pi_u \rightarrow B^3\pi_g$

λ	v', v''	λ	v', v''	λ	v', v''
4649·4	4, 10	3998·4	1, 4	3371·3	0, 0
4574·3	1, 6	3943·0	2, 5	3339	1, 1
4490·2	2, 7	3894·6	3, 6	3309	2, 2
4416·7	3, 8	3804·9	0, 2	3285·3	3, 3
4343·6	0, 4	3755·4	1, 3	3268·1	4, 4
4269·7	1, 5	3710·5	2, 4	3159·3	1, 0
4200·5	2, 6	3671·9	3, 5	3136·0	2, 1
4141·8	3, 7	3576·9	0, 1	3104·0	4, 3
4059·4	0, 3	3536·7	1, 2	2962·0	3, 1
		3500·5	2, 3	2953·2	4, 2

The fourth positive system $D^3\Sigma_u^+ \rightarrow B^3\pi_g$

λ	v', v''
2660·5	0, 4
2550·7	0, 3
2448·0	0, 2
2351·4	0, 1

TABLE 1. Observed band heads in vortex glow. λ, Wavelength in microns; v', v'', vibrational quantum numbers in the higher and lower states, respectively.

System	Upper state energy	Transition energy
1st pos. N_2	$B^3\pi_g(v = 8)$; 8·9 eV	$B^3\pi_g \rightarrow A^3\Sigma_u^+(8, 5)$; 1·9 eV
2nd pos. N_2	$C^3\pi_u(v = 4)$; 11·9 eV	$C^3\pi_u \rightarrow B^3\pi_g(4, 2)$; 4·1 eV
4th pos. N_2	$D^3\Sigma_u^+(v = 0)$; 12·7 eV	$D^3\Sigma_u^+ \rightarrow B^3\pi_g(0, 1)$; 5·2 eV

TABLE 2. Upper state and transition energies of the observed systems.

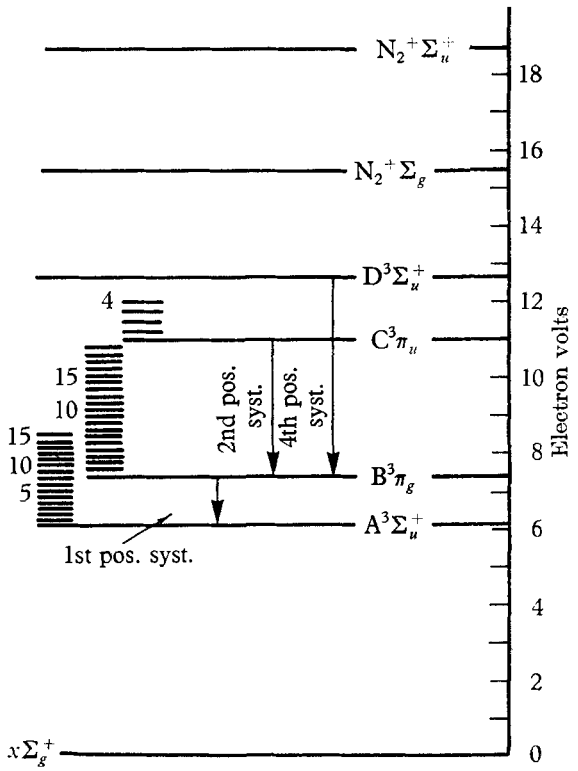

FIGURE 6. Energy level diagram of the first, second and fourth positive N_2 systems (after Herzberg 1950).

4. Electrical circuitry

The absence of luminescence in ducts made of conducting materials points to electrostatic charges on the surface of the dielectric wall as a likely cause of the phenomenon. A scheme was thus devised to examine the axial distribution of these charges. As shown in figure 7, it is essentially a capacitive voltage-divider circuit consisting of a large polystyrene capacitor, C_e, and of the capacitor, C_p, formed by the test section. The wall of the test section is the dielectric, the charge-carrying inner duct surface represents one of the conducting plates and aluminium foil wrapped around the outside of the test section forms the second plate.

Local charging currents were detected by sensing probes made of $\frac{5}{8}$ in. wide sections of the aluminium foil separated by $\frac{1}{16}$ in. gaps from the rest of the wrapping which was grounded. The probes were centred at distances of 6·25, 10·75 and 15·5 in. from the upstream end of the test section; their capacitances were 25·0, 25·2 and 25·9 $\mu\mu$F. The charging currents were measured by Keithley electrometers; their output signals were displayed on dual beam Tektronix oscilloscopes.

The probes were maintained at near ground potentials and since C_p/C_e was much less than unity, the charging current and the electric potential of the inner duct wall could be obtained with sufficient accuracy from simple approximate relationships. The accuracy of the measurements was $\pm 5\,\%$ when the charging current exceeded 10^{-12} amp.

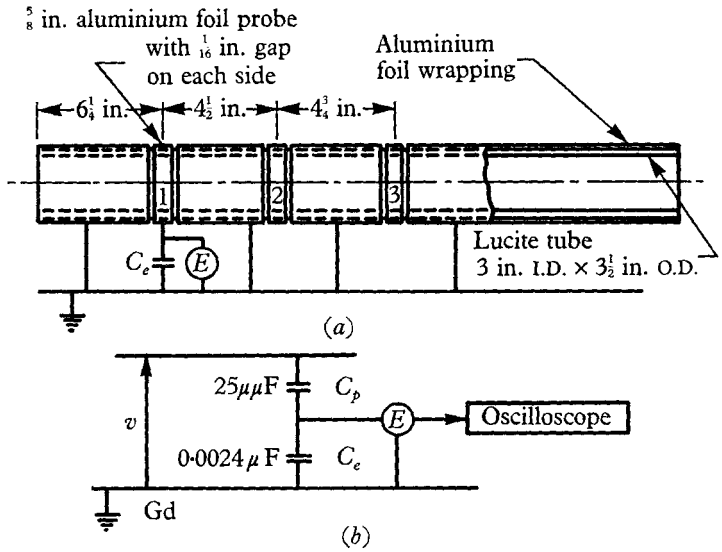

FIGURE 7. Charging-current sensing probes. (*a*) Physical arrangement. (*b*) Equivalent electric circuit.

5. Build-up of the electric field

At low specific humidities, the measured charging current to the probes was uniform, suggesting that the charging is due to particles with large mass-to-

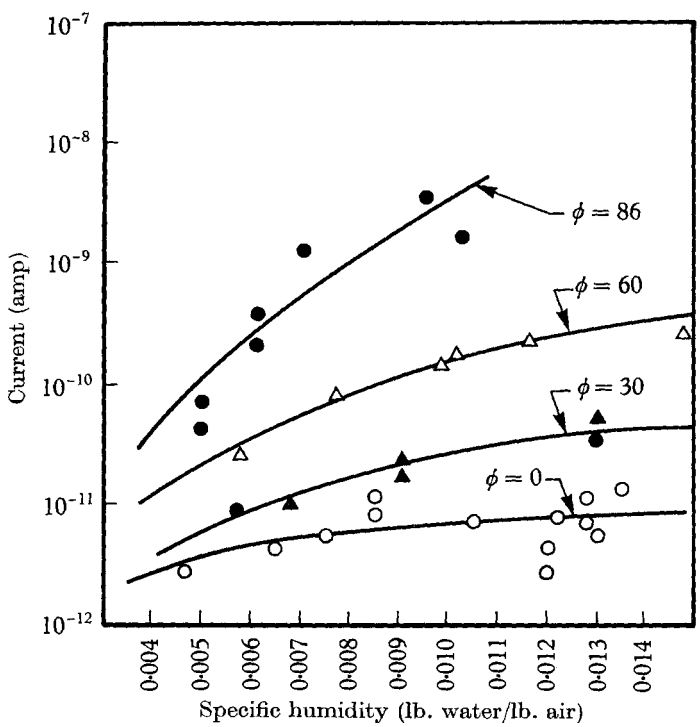

FIGURE 8. Probe charging current as a function of specific humidity, with swirl angle as a parameter (ϕ is the pre-rotation vane setting).

charge ratios, whose motion could not be affected appreciably by electric fields. At a specific humidity of, say 0·0061, the measured charging current was $4{\cdot}4 \times 10^{-10}$ amp; the electric potential on the inner wall reached a value of 830 V in 47 sec. The relatively slow rate of potential build-up was achieved by increasing the capacitance of the test section wall using the aluminium wrapping. This feature made it possible to observe conveniently the rate of charge build-up preceding the onset of discharge without otherwise affecting the phenomenon.

The charging current sensed by one of the probes at several values of specific humidity and pre-rotation vane setting is plotted in figure 8. The current intensities vary from 10^{-12} to 5×10^{-9} amp, representing a rate of increase of the electric potential on the inner wall of 0·04–200 V/sec.

6. Conditions during discharge

At high electric field intensities, when glow discharge was present, the probe charging rates exhibited a random, slowly oscillating pattern with a fine structure superimposed on it. These high-frequency fluctuations were displayed on one of the oscilloscope channels which was connected for this purpose directly to the sensing probes. The resulting traces were compared with the glow intensity fluctuations in the 4000 Å band. These were transmitted to the second channel of the oscilloscope using a Hilger monochrometer coupled with an IP-28 photomultiplier tube. It is apparent from figure 9(*a*) (plate 2) that the two fluctuations are in phase and that the light output is intermittent, suggesting a power-limited discharge mechanism. Traces of the same phenomenon taken at lower sweep rates are shown in figure 9(*b*) (plate 2). These show that light is emitted at both positive and negative probe potentials but only during periods of potential increase.

The magnitude of the current fluctuations cannot be ascertained from these records because of the amplitude attenuation caused by the relatively low impedance of the oscilloscope. However, charging-current measurements reveal that the order of magnitude of the changes in probe potential during the fluctuations (figure 9(*a*)) is insignificant compared with the decrease of $\sim 50\ \%$ required for an intermittent gas discharge (Francis 1956; Meek & Craggs 1953).

On the basis of the preceding considerations, it appears that the glow discharge is maintained by an intermittent build-up and neutralization of negative space charges in the interior of the duct. During the neutralization phase, which is registered by the probes as a net potential increase, light is emitted (figure 9).

7. The charging mechanism

Based on the data yielded by this study, a causal relationship has been established between the luminescent space discharge and the charge distribution on the inner wall of the test section. The origin of these charges will now be considered.

It has been found that the charging rate is extremely low when the air entering the apparatus is dry and that it increases by orders of magnitude with an increase in relative humidity. Furthermore, injection of water into the centre of the passage cross-section resulted in a rapid increase in charging rate and subse-

quent glow discharge identical to that observed in high-humidity flows. On the other hand, direct wetting of the test section walls did not produce such effects. It appears, therefore, that the charging mechanism is based primarily on condensed water droplets and, to a much smaller extent, on dust and other impurities. These particles are accelerated radially outward by the swirl and impinge on the test section, charging it positively.

From the equations of motion of water droplets with the drag forces calculated from Stokes's law, it has been determined that water particles smaller than 8μ pass through the test section without reaching the wall, while the larger drops impinge on the wall with velocities of the order of 300 ft./sec. As smaller droplets are, on the average, negative, while larger ones carry statistically a positive charge (Loeb 1958), the centrifugal field results in an accumulation of positive charges on the wall. The efficiency of this charge-separation mechanism can be estimated by assuming that all of the water vapour entering the test section condenses. Thus, at a specific humidity of 0·01, the measured rate of charge accumulation on the test section wall was 3×10^{-7} C/sec, corresponding to a charge separation efficiency of 10^{-7} C/g of water. This value is two orders of magnitude larger than those observed in studies of charge separation in water sprays and one order of magnitude larger than the theoretical limit estimated by Loeb.

8. Conclusion

The reported measurements and observations made prior to the onset of glow discharge and during discharge lead to the following explanation of the nature of this phenomenon.

Water droplets formed in the supersonic nozzle during the rapid expansion of humid air are entrained by the swirling flow entering the test section. The larger droplets impinge on the test section wall, distributing, in the process, positive charges on the surface. These charges produce a strong electric field in the test section. When the intensity of the field reaches a certain level, glow discharge ensues. The emission spectrum of this glow is identical with spectra of the positive column of nitrogen discharge tubes. The observed dependence of glow intensity on specific humidity and swirl velocity and the intermittent nature of the glow are, thus, readily explained.

The finding that the glow is more intense near an axial Mach number of two than at lower and higher Mach numbers is also in accord with the above explanation. At the higher Mach numbers nozzles of smaller throat diameter were used, resulting in lower flow rates, thereby causing a decrease in the number of droplets reaching the wall. On the other hand, the smaller nozzle expansion ratios associated with lower Mach numbers hindered condensation of the water vapour.

This research was performed under Contract No. AF 33–615–1031 for Aerospace Research Laboratories, Office of Aerospace Research, Dayton, Ohio. Acknowledgement is also due to Messrs Mark Cann and Henry Seiwatz for their assistance in various phases of the work. The study was made in partial fulfilment of the requirements for the degree of Doctor of Philosophy of the first author in the graduate school of Illinois Institute of Technology.

REFERENCES

DOBRATZ, B. M. 1964 Vortex tubes, a bibliography. *TID* 4500 (29th ed.), Lawrence Radiation Laboratory, University of California.

FRANCIS, G. 1956 The glow discharge at low pressure. *Handbuch der Physik*, vol. 22, p. 53. Berlin: Springer.

GARTSHORE, I. S. 1962 Recent work in swirling incompressible flow. *Aero. Rep. LR*-343, *Nat. Res. Counc. Canada.*

HERZBERG, G. 1950 *Molecular Spectra and Molecular Structure.* I. *Spectra of Diatomic Molecules.* Princeton: Van Nostrand.

HOWARD, L. 1953 *Modern Development in Fluid Dynamics; High Speed Flow*, vol. I. Oxford: Clarendon Press.

LOEB, L. B. 1958 *Static Electrification.* Berlin: Springer.

MEEK, J. M. & CRAGGS, J. D. 1953 *Electrical Breakdown of Gases.* Oxford: Clarendon Press.

MILNE-THOMPSON 1957 *Theoretical Hydrodynamics.* New York: MacMillan.

PEARSE, R. W. B. & GAYDON, A. G. 1941 *The Identification of Molecular Spectra.* New York: Wiley.

RANQUE, C. J. 1933 Experiences sur la detente giratoire avec productions simultanees d'un echappement d'air chaud et d'un echappement d'air froid. *J. Phys. & Radium*, **4**, 112S-115S.

STICKNEY, T. M. 1955 Recovery and time-response characteristics of six thermocouple probes in subsonic and supersonic flow. *NACA TN* no. 3455.

WESTLEY, R. 1954 *A Bibliography and Survey of the Vortex Tube.* College of Aeronautics, Cranfield.